

Characterization and Electrochemical Behavior of Graphene-Based Anode for Li-Ion Batteries

Wei-Ren Liu^{*,1,2}, Shin-Liang Kuo¹, Chia-Yi Lin², Yi-Chen Chiu¹, Ching-Yi Su¹, Hung-Chun Wu¹ and Chien-Te Hsieh^{*,3}

¹Material and Chemical Research Laboratories, ITRI, Hsinchu 300, Taiwan, R.O. China

²Department of Chemical Engineering, Chung Yuan Christian University, 200, Chung Pei Rd., Chung Li, 32023, Taiwan, R.O. China

³Department of Chemical Engineering and Materials Science, Yuan Ze Fuel Cell Center, Yuan Ze University, Taoyuan 320, Taiwan, R.O. China

Abstract: In this study, we investigate the characteristics and electrochemical properties of graphene nanosheets derived from chemical-thermal exfoliation processes of SFG44 synthetic graphite (SFG44-GNS). The characterizations and electrochemical measurements were carried out by means of X-ray diffraction, scanning electron microscopy, transmission electron microscopy, cyclic voltammetry, BET, Raman, rate capability as well as cycling tests and AC impedance. The as-synthesized SFG44-GNS with larger d-spacing of 0.3407 nm exhibits reversible capacity of 626 mAh/g and good rate capability of ~300 mAh/g at 2C rate, which are superior to those of graphite anode. The enhanced electrochemical performance of GNS anode was resulted from larger d-spacing, lower impedance in the interface and enhanced pore volume. The results indicate that graphene-based material is a good candidate for HEV/EV application.

Keywords: Graphene, Anode, Li-ion battery, Exfoliation.

1. INTRODUCTION

Graphene, one atom thick two dimensional layers of sp²-bonded carbon, has been emerging as a fascinating material with many unusual physical, chemical and mechanical properties. Thus, much attention has been drawn in technology applications, such as solar cells, hydrogen storage, supercapacitors and batteries [1-5]. Among these energy storage systems, lithium-ion batteries (LIB) are currently the predominant power sources for portable electronic devices and electrical/hybrid vehicles. Graphite is widely used as an anode material for commercial rechargeable LIBs due to its excellent cycle life. However, lower theoretical capacity of 372 mAh g⁻¹ and poor rate capability limit its application on electrical/hybrid vehicles. Recently, a new kind of carbon material, graphene (or graphene nanosheets, namely GNS) obtained from exfoliation of graphite by chemical method, might be a potential alternative anode materials for LIB applications. Such as Paek *et al.*, [6] and Yao's group [7] reported SnO₂/graphene composites delivered a reversible capacity of 810 mAh g⁻¹ and 765 mAh g⁻¹, respectively. Yoo *et al.*, [8] studied the electrochemical performance of graphene/CNT and graphene/C₆₀ composites, of which the capacities were 730 mAh g⁻¹ and 780 mAh g⁻¹, respectively. Wang *et al.*, discussed the application of GNS as an anode material, giving a reversible capacity of 650 mAh g⁻¹ in the first cycle [9]. Chou *et al.*, demonstrated nanosize

silicon/graphene composite anode with 1:1 wt. ratio showed a high capacity of 2158 mAh/g in the first cycle and 1168 mAh g⁻¹ after 30 cycles [10].

Here, we report the rate capability of graphene nanosheets synthesized by modified Hummer's method. Their corresponding crystal structure, surface morphology, cycling tests, as well as AC impedance were discussed in this study.

2. EXPERIMENTAL

2.1. Samples Preparation

Graphene nanosheet (SFG44-GNS) derived from SFG44 synthetic graphite powders (TIMCAL®) were synthesized by the modified Hummers' method¹¹ described in detail as follows: 8g graphite powder and 4 g NaNO₃ were put into 560 ml concentrated H₂SO₄ solution with stirring for 2 hours. Then 24g KMnO₄ was gradually added into the flask with ice bath for 2 hours. The mixture was diluted by 800 ml de-ionized water (DI water). After that, 5% H₂O₂ was added into the solution until the color of the mixture changed to brown, indicating fully oxidized graphite was obtained. The as-obtained graphite oxide slurry was re-dispersed in DI water. Then, the mixture was washed by 0.1M HCl solution to remove SO₄²⁻ ions. Finally, the product was washed with DI water to remove the residual acid until the pH was reached to ~7. By cleaning with DI water, filtrating and drying in vacuum for 24 h (the obtaining powders were graphene oxide, namely SFG44-GO). The GO powder was subsequently reduced at 300°C for 2 hours under a reducing atmosphere of 15%H₂/85%N₂, namely SFG44-GNS-300.

*Address correspondence to these authors at the Material and Chemical Research Laboratories, ITRI, Hsinchu 300, Taiwan, R.O. China; Fax: +886-3-5723764; E-mail: WRLiu@itri.org.tw and Department of Chemical Engineering and Materials Science, Yuan Ze Fuel Cell Center, Yuan Ze University, Taoyuan 320, Taiwan, R.O. China; E-mail: cthsieh@staurn.yzu.edu.tw

2.2. Electrodes Preparations

The composite electrode consists of 89 wt.% SFG44-GNS-300, 1 wt.% Super-P (40nm, TIMCAL) as conductive additive and 10 wt.% water-based-binders of SBR and CMC [12]. The mixed-slurry was coated on Cu-foil with a final film thickness of $\sim 50 \mu\text{m}$. CR2032 coin cells were fabricated from the electrode for electrochemical characterizations. The bare SFG44 graphite electrode was prepared in the same way. The counter electrode is lithium foil. The electrolyte is 1M LiPF₆ in ethylene carbonate (EC): ethyl methyl carbonate (EMC) (1:2 vol. %) from Mitsubishi. All the potentials reported herein are referenced to Li. The current densities refer to masses excluding binder and conductive additives.

2.3. Characterizations

Cyclic voltammetry (CV) analysis was performed between 0.05 V to 3.0 V at 5 mV/min. The charge/discharge (C/D) tests were carried out with a constant-current-constant voltage (CC-CV) mode within the voltage range from 0.001 to 3.5 V. The CC process employed a current of 0.1 mA/mg, while the CP process was fixed to 0.001V with a cut-off current of 0.03 mA/mg. The morphologies of the synthesized graphene material were examined by scanning electron microscopy (SEM; LEO1530). Transmission electron microscopy (TEM) analysis was conducted with a field-emission transmission electron microscope (FE-TEM, JEOL JEM-2100F). X-ray diffraction (XRD) was carried out on a Mac-Science/MXP diffractometer with CuK α radiation. Thermal gravimetric analysis (TGA) was performed by using an Ulvac TGD-7000 at a scanning rate of 10°C min⁻¹.

3. RESULTS AND DISCUSSION

3.1 Thermogravimetric Analysis and Crystal Structure of Graphene-Based Materials

Fig. (1) shows the TGA and its derivative curves of SFG44-GO with a heating rate of 10 °C/min in inert atmosphere. Two apparent weight loss at 33°C and 216°C were observed in SFG44-GO, which might be attributed to the desorption of adsorbed water and decomposition of functional groups including hydroxyl and carboxylic groups, respectively. The result indicates that the functional groups derived from oxidative exfoliation process could be almost eliminated by post heating process as long as the temperature is above 300°C.

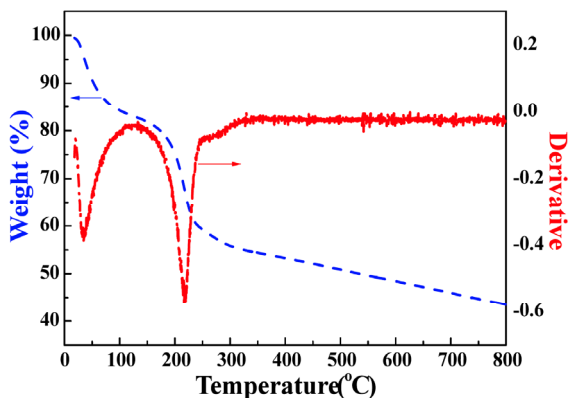


Fig. (1). TGA curves of SFG44-GO with a heating rate of 10 °C/min.

Fig. (2) displays the XRD patterns of bare SFG44, SFG44-GO and SFG44-GNS-300, respectively. Before exfoliation treatment, highly crystalline SFG44 give a sharp diffraction peaks, of which crystallite size exceeding 30 nm determined by Scherrer equation. The d-spacing of SFG44 could be calculated to be 0.335 nm according to (002) reflection. After exfoliation and oxidation by modified Hummer's method, the obtained SFG44-GO showed a typical diffraction peak at 12° ($d_{002} \sim 7.4 \text{ \AA}$). SFG44G, being reduced with hydrazine, almost showed amorphous nature, of which average d-spacing could be roughly determined as 0.375 nm.; in the meanwhile, 300°C calcined sample (SFG44-GNS-300) showed a larger d-spacing to 0.3407 nm and amorphous nature. These properties are similar to that of hard carbon, which may good for reversible capacity and rate capability.

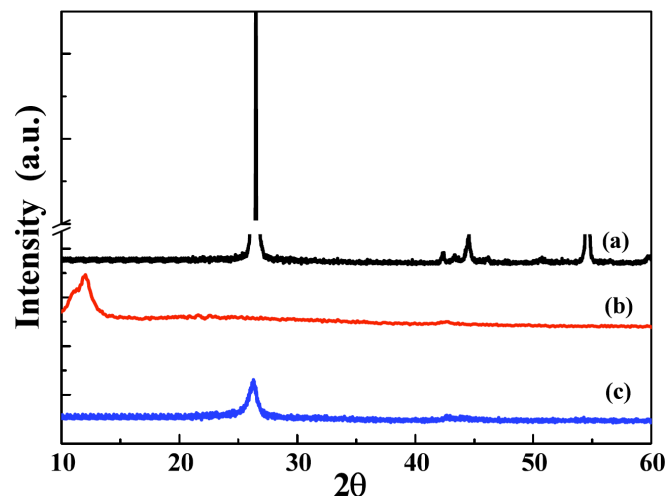


Fig. (2). XRD patterns of (a) bare SFG44; (b) SFG44-GO; (c) SFG44-GNS-300.

3.2. Surface Morphologies and Cross-Section Images of Graphene-Based Materials

The SEM micrographs of SFG44 and SFG44-GNS-300 are shown in Fig. (3A, B), respectively. SFG44 graphite is a flake-like structure with very dense nature on the surface. SFG44-GNS-300, on the other hand, displayed a flower-like morphology with porous structure, in which the penetration of both electrolyte and Li-ion would be much easier. The porous structure SFG44-GNS-300 with fewer layers could provide not only additional sites for lithium ions, but also to occupy and facilitate the kinetics of lithium for insertion/extraction. Fig. (4A, B) illustrates the TEM micrographs of SFG44 and SFG44-GNS-300. The d_{002} and graphene layers of SFG44 were $\sim 0.332 \text{ nm}$ and ~ 100 layers, respectively. After exfoliation process, d-spacing and thickness of SFG44-GNS-300 were observed to be 0.352 nm $\sim 0.511 \text{ nm}$ and 10~40 layers, respectively. The inset in Fig. (4B) displays the SEM micrograph giving a soft and flexible nature due to the thickness of graphite could be efficiently reduced by exfoliation process.

3.3. Raman and BET Analyses of Graphene-Based Materials

Fig. (5) shows Raman spectra of bare SFG44, SFG44-GO and SFG44-GNS-300. Raman spectroscopy is a direct and non-destructive measurement for characterization of

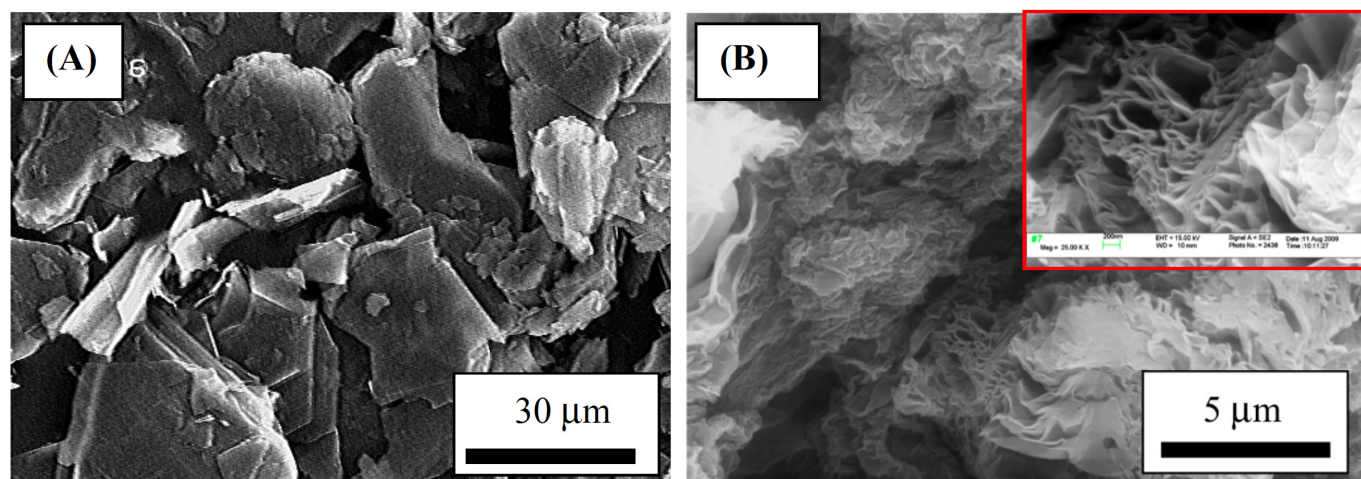


Fig. (3). SEM micrographs of graphite w/o exfoliation process: (A) bare SFG44; (B) SFG44-GNS-300. The inset: larger magnitude image of SFG44-GNS-300.

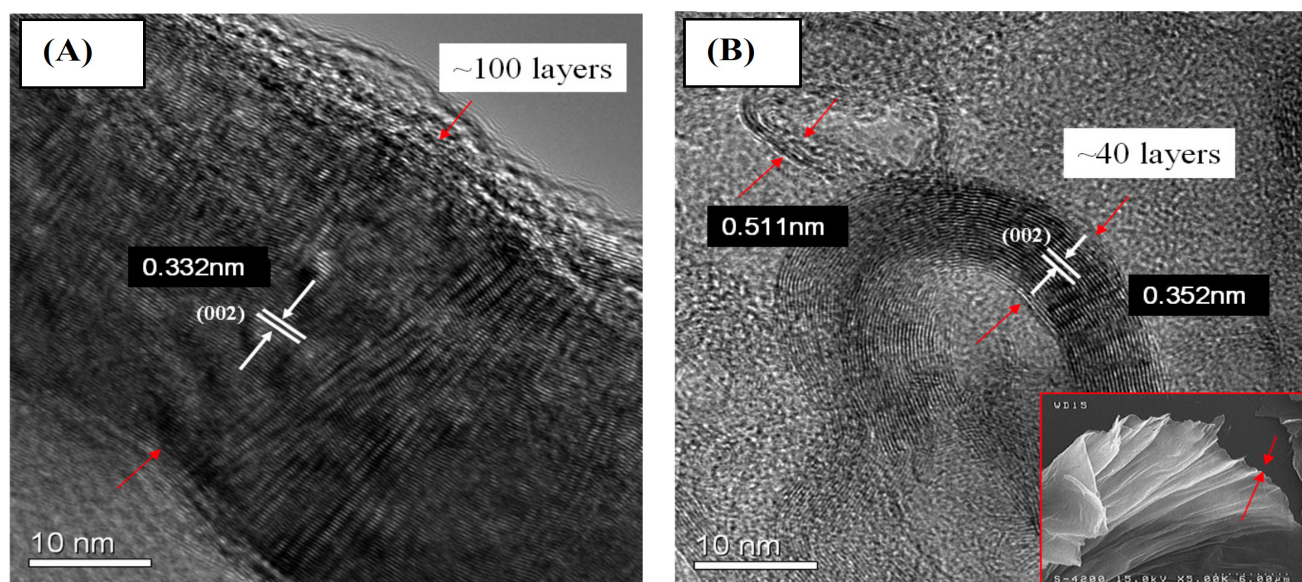


Fig. (4). (A) TEM micrographs of the SFG44 and (B) SFG44-GO. The inset shows the graphene with soft nature.

disorder structure of graphitic materials. Two characteristic peaks generally named by D ($\sim 1355 \text{ cm}^{-1}$) and G ($\sim 1580 \text{ cm}^{-1}$) bands were observed in graphite-based materials. The G band represents the first order scattering of the E_{2g} photons observed for sp^2 carbon domain, while the D band corresponds to breathing mode or j-point photons of A_{1g} symmetry associated with disorder band of structural defect, amorphous carbon or edge. The intensity ratio of D band to G band (I_D/I_G) is usually used as a measure of disorder. In comparison to bare graphite, both SFG44-GO and SFG44-GNS-300 showed broader G band accompanying with board D band, indicative of a highly disorder in graphitic structure. It shows that even most functional groups were removed by the reduction process, the sp^3 could not be restored to original sp^2 graphitic structure. In addition, there is no significant decrease in I_D/I_G ratio for graphene nanosheets after high temperature reduction, even re-crystallization process was observed in XRD patterns. It is indicative of the functional groups derived from oxidation process could be removed but sp^3 dangling bond could not be restored to original sp^2 graphene structure.

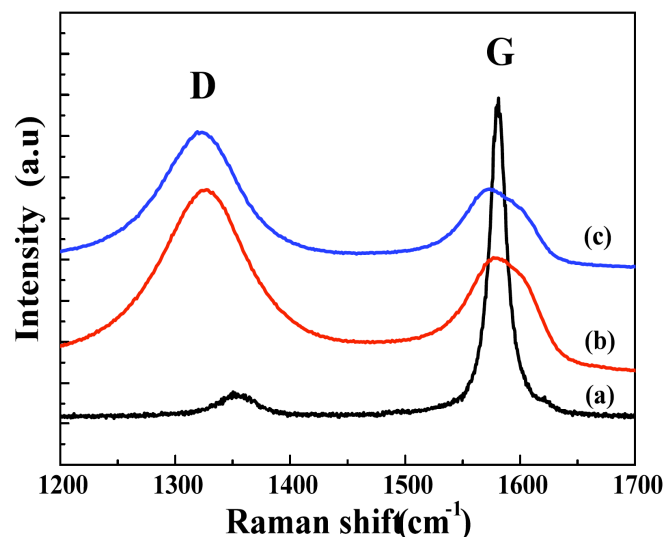


Fig. (5). Raman spectra of (a) bare SFG44, (b) SFG44-GO and (c) SFG44-GNS-300.

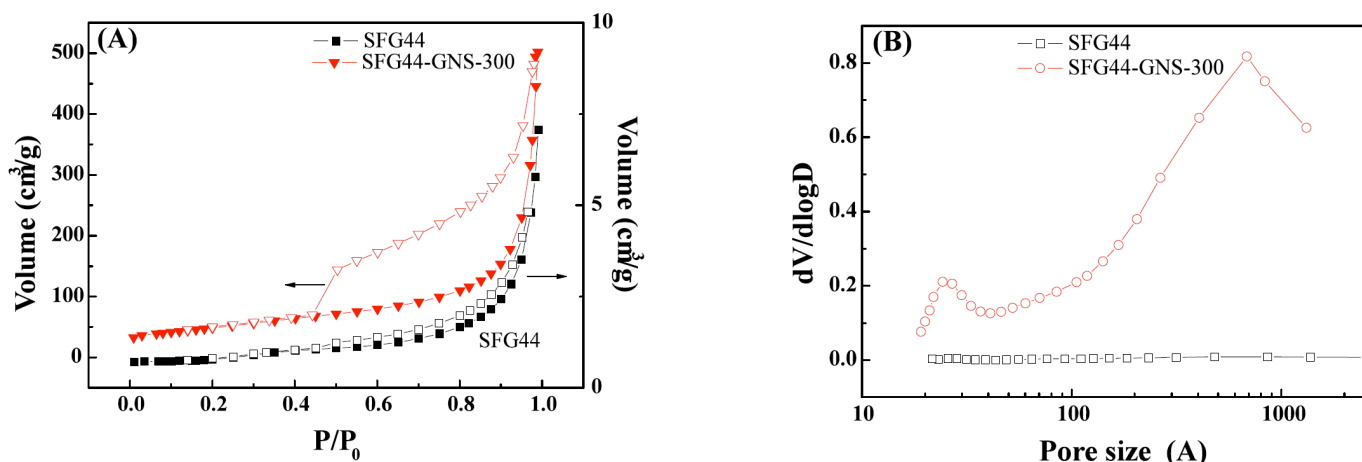


Fig. (6). (A) Isotherm adsorption/desorption curves of bare SFG44 and SFG44-GNS-300; (B) Pore size distribution of as-bare SFG44 and SFG44-GNS-300.

Fig. (6A) shows isotherms and pore size distributions of SFG44 and SFG44-GNS-300. The BET surface area of SFG44 graphite was $2.61 \text{ m}^2 \text{ g}^{-1}$. By exfoliation process, the BET of SFG44-GNS-300 could be dramatically enhanced by $171 \text{ m}^2 \text{ g}^{-1}$. The value of BET for SFG44-GNS-300 is much smaller than theoretical value of graphene of $2620 \text{ m}^2 \text{ g}^{-1}$, indicative of SFG44-GNS-300 sample was not fully exfoliated to single layer graphene instead of few-layers graphene. The BJH pore size distributions were shown in Fig. (6B). The main pore size belongs to meso-pore, where the micro pore portion was not dominant. The larger BET and pore volume could not only provide additional sites for Li-ion to occupy, but also facilitate the kinetics of Li intercalation/extraction processes.

3.4. Electrochemical Tests of Graphene-Based Materials

Fig. (7A, B) show the CV curves of SFG44 and SFG44-GNS-300 at the first second cycles. The CV curves of SFG44 exhibited a typical sharp reduction/oxidation peaks at $\sim 0.15 \text{ V}$ and 0.23 V , respectively. After exfoliation, the electrochemical behavior definitely differed from that of graphite. The reduction/oxidation peaks become much broader in the first two cycles in Fig. (6B). The lithium-intercalation reactive potential increased from $\sim 0.15 \text{ V}$ to $\sim 0.6 \text{ V}$, which indicates the kinetics of lithium and graphene

was higher than that of graphite. In other words, the energy barriers of diffusion and reaction of Li/C were lower for graphene anodes compared to graphite. For de-intercalation process, two broad humps peaking between 0.01 V to 3.0 V were observed in Fig. (7B). The higher potential of de-intercalation could be responsible for some lithium ions were tightly trapped in the structure defects due to the amorphous nature of graphene.

Fig. (8A, B) shows the C/D curves of SFG44 and SFG44-GNS-300 in the first two cycles. The 1st and 2nd reversible capacity of SFG44 were 334 mAh g^{-1} and 327 mAh g^{-1} , respectively; in the meanwhile, the irreversibility of the 1st cycle was 21.7%. The discharging plateau (lithium-insertion) of SFG44 was observed to be $\sim 0.05 \text{ V}$, which is graphite-like behavior. On the other hand, SFG44-GNS-300 showed the extremely high reversible capacities, 626 mAh g^{-1} and 561 mAh g^{-1} for the 1st and 2nd cycle, and irreversibility of the 1st cycle is about 51.9%. Yoo *et al.*, demonstrate that the layer of graphene is a function of d-spacing as well as charge capacity [8]. In our case, the average d-spacing of as-synthesized graphene is $\sim 0.375 \text{ nm}$ estimated by XRD. According to fitting data of Yoo's group, the reversible charge capacity of as-synthesized graphene is around 600 mAh g^{-1} , which is in consistent with our results.

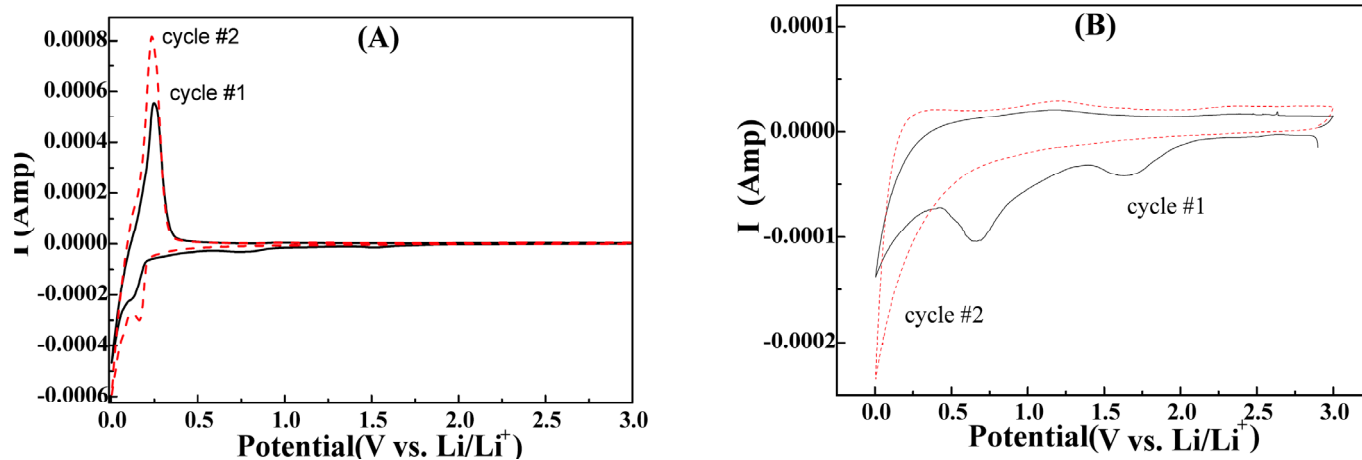


Fig. (7). CV curves of graphite w/o exfoliation process for the first two cycles: (A) SFG44; (B) SFG44-GNS-300.

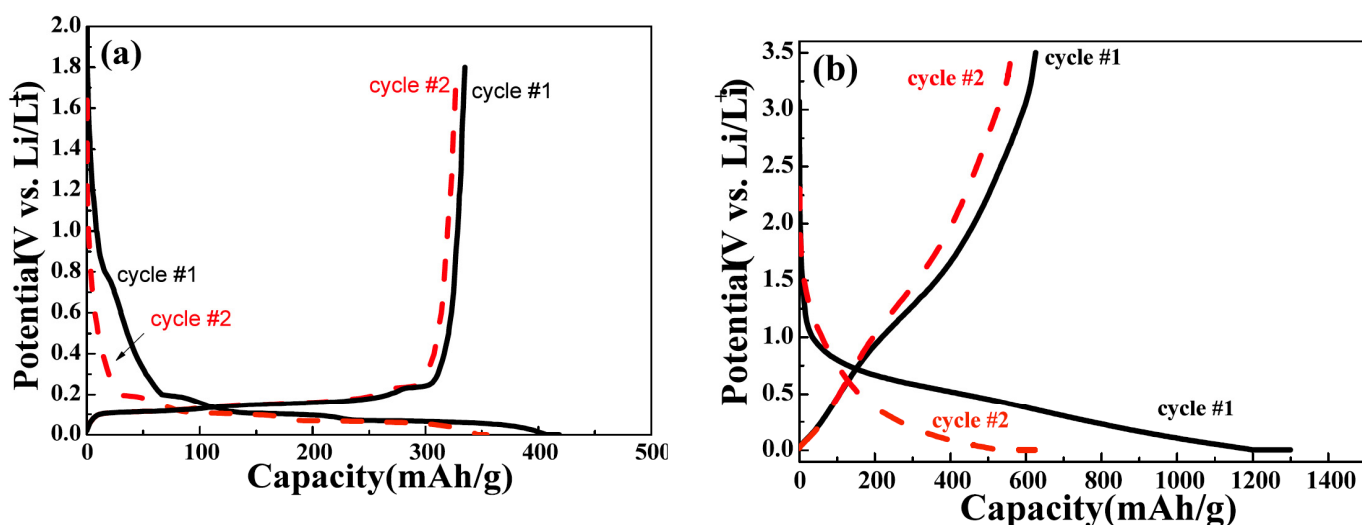


Fig. (8). Charge/discharge curves in the first two cycles at 0.1C: (a) SFG44 and (b) SFG44-GNS-300.

Nevertheless, the large irreversible capacity loss of graphene-based anode in the first cycle was also reported by many groups in the range of 50–80%. The possible reasons could be ascribed to (i) larger specific surface area; (ii) structure defects; (iii) function groups and (iv) SEI (solid electrolyte interface). The reducing of irreversible capacity loss for graphene-based anode materials would be the most important issue for their application on LIBs. In the present results, the irreversible capacity loss of graphene was mainly attributed to higher surface area, structure defects and SEI. Which is the main factor is worthy to discuss in the future work.

Fig. (9) shows the cycling tests of SFG44 and SFG44-GNS-300 for 30 cycles with charging/discharge currents of 0.2C. SFG44 graphite gave a reversible capacity of ~ 334 mAh g^{-1} with fair cyclability. The SFG44-GNS-300 sample, on the other hand, exhibited ~ 600 mAh g^{-1} in the first cycle and retained 280 mAh g^{-1} after 30 cycles. The inset of Fig. (9) displays the charge capacity of SFG-44 and SFG44-GNS-300 with different C rates. With 2C discharge, the capacity of SFG44-GNS-300 is as high as 300 mAh g^{-1} ($\sim 50\%$ of 0.2C). The capacity of SFG44 graphite is only 75

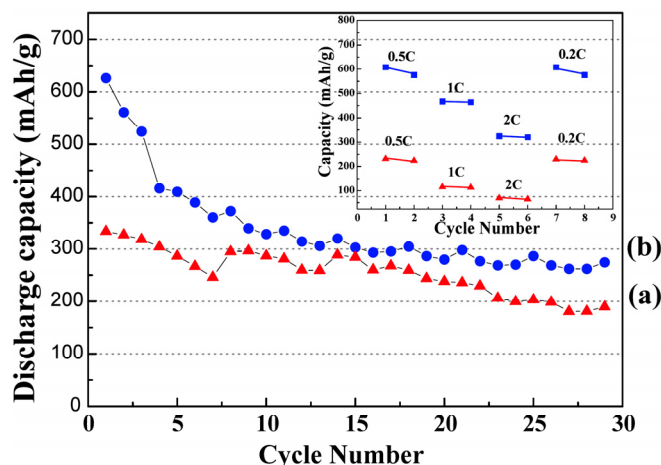


Fig. (9). Cycling tests of SFG44 (a) and SFG44-GNS (b) at 0.2C. The inset shows their rate capability.

mAh g^{-1} at 2C ($\sim 22\%$ of 0.2C). The results surprisingly showed that the SFG44-GNS-300 exhibited better rate capability than that of graphite sample. The impedance data of these two samples in discharging state of 0.01V at the 4th cycle are shown in Fig. (10). The result future demonstrated that the charge transfer resistance of SFG44-GNS-300 was lower than that of SFG44 graphite, which indicates that the good rate capability could be explained by the lower impedance for SFG44-GNS-300. Thus, the graphene-based anode materials might be good anode materials for EV or HEV applications due to their good performance with high rate charge/discharge tests.

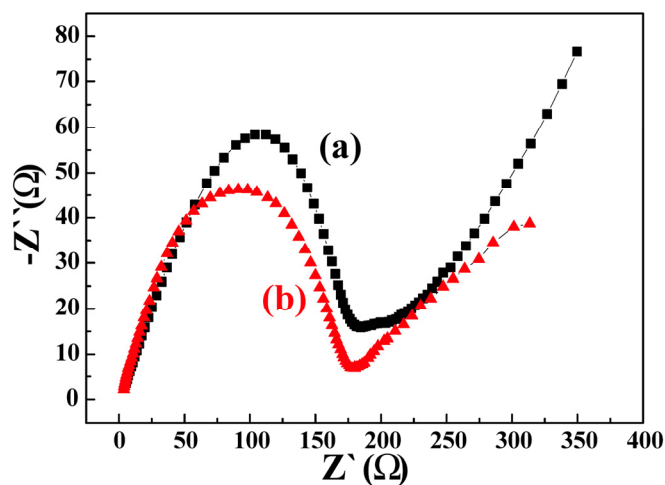


Fig. (10). AC impedance spectra for SFG44 (a) and SFG44-GNS-300 (b) with discharging state of 0.01V at the 4th cycle.

CONCLUSIONS

In summary, SFG44-GNS-300 is synthesized by modified Hummers' method. The relationship between electrochemical performance, such as reversible capacity, rate capability and irreversible capacity, and structure characterization of BET, pore distribution and surface morphology, are discussed by means of charge/discharge tests, rate capability tests, BET, as well as Raman spectroscopy and XRD measurements. These corresponding results could be the reference for structure design of

graphene-based anode for the application of Li-ion batteries in the future.

ACKNOWLEDGEMENTS

The work is financially supported from ITRI under contract no. A301AR4830 and the NSC (contract no. NSC96-2221-E-155-055-MY2-2).

REFERENCES

- [1] Idota Y, Kubota T, Matsufuji A, Maekawa Y, Miyasaka T. Tin-based amorphous oxide: a high-capacity lithium-ion-storage material. *Science* 1997; 276: 1395-7.
- [2] Maier J. Nanoionics: ion transport and electrochemical storage in confined systems. *Nat Mater* 2005; 4: 805-15.
- [3] Loi XW, Wang Y, Yuan C., Lee JY, Archer LA. Template-free synthesis of SnO₂ hollow nanostructures with high lithium storage capacity. *Adv Mater* 2006; 18: 2325.
- [4] Chan CK, Zhang XF, Cui Y. High capacity Li-ion battery anodes using Ge nanowires. *Nano Lett* 2008; 8: 307-9.
- [5] Kim DW, Hwang IS, Kwon SJ, *et al.* Highly conductive coaxial SnO₂-In₂O₃ heterostructured nanowires for li-ion battery electrodes. *Nano Lett* 2007; 7: 3041-5.
- [6] Paek SM, Yoo E, Honma I. Enhanced cyclic performance and lithium storage capacity of SnO₂/graphene nanoporous electrodes with three-dimensionally delaminated flexible structure. *Nano Lett* 2009; 9: 72-5.
- [7] Yao J, Shen X, Wang B, Liu H, Wang G. *In situ* chemical synthesis of SnO₂-graphene nanocomposite as anode materials for lithium-ion batteries. *Electrochem Commun* 2009; 11: 1849-52.
- [8] Yoo E, Kim J, Hosono E, Zhou HS, Kudo T, Honma I. Large reversible Li storage of graphene nanosheet families for use in rechargeable lithium ion batteries. *Nano Lett* 2008; 8: 2277-82.
- [9] Wang G, Shen X, Yao J, Park J, Graphene nanosheets for enhanced lithium storage in lithium ion batteries. *Carbon* 2009; 47: 2049-53.
- [10] Chou SL, Wang JZ, Choucair M, Liu HK, Stride JA. Enhanced reversible lithium storage in a nanosize silicon/graphene composite. *Electrochem Commun* 2010; 12: 303-6.
- [11] Hummers WS, Offeman RE, Preparation of graphitic oxide. *J Am Chem Soc.* 1958; 80: 1339.
- [12] Liu WR, Yang MH, Wu HC, Chiao SM, Wu NL. Enhanced cycle life of Si anode for li-ion batteries by using modified elastomeric binder. *Electrochem Solid State Lett* 2005; 8: A100-3.

Received: October 19, 2010

Revised: May 25, 2011

Accepted: June 23, 2011

© Liu *et al.*; Licensee Bentham Open.

This is an open access article licensed under the terms of the Creative Commons Attribution Non-Commercial License (<http://creativecommons.org/licenses/by-nc/3.0/>) which permits unrestricted, non-commercial use, distribution and reproduction in any medium, provided the work is properly cited.